Fe on W(001) from continuous films to nanoparticles: Growth and magnetic domain structure

Y. R. Niu,[1,*] K. L. Man,[1,†] A. Pavlovska,[2] E. Bauer,[2] and M. S. Altman[1]
[1]*Department of Physics, Hong Kong University of Science and Technology, Hong Kong SAR, China*
[2]*Department of Physics, Arizona State University, Tempe, Arizona 85287, USA*
(Received 21 October 2016; revised manuscript received 7 January 2017; published 6 February 2017)

The evolution of the structural and magnetic properties of Fe films during growth on the W(001) surface have been studied with low energy electron diffraction, real-time low energy electron microscopy, and quasi-real-time, spin-polarized low energy electron microscopy in the absence of a magnetic field (virgin state). Depending on the growth temperature, different growth modes are observed: growth of atomically rough and highly strained (10.4% tensile) pseudomorphic films at room temperature, kinetically limited layer-by-layer growth (quasi–Frank-van der Merwe growth mode) of smooth pseudomorphic films up to 4 monolayers at around 500 K and growth of fully relaxed three-dimensional Fe islands on top of a thermodynamically stable 2-monolayer-thick wetting layer (Stranski-Krastanov growth mode) at and above 700 K. Around 500 K, layered growth is terminated by partial (2 monolayers) dewetting of the metastable Fe film and formation of thin, partially relaxed, elongated islands on a thermodynamically stable 2 monolayer film. Ferromagnetic order is first detected during growth at room temperature at 2.35 monolayer Fe film thickness. The magnetization is in-plane with a thickness-dependent direction, rotating from the substrate ⟨110⟩ directions at 3 monolayers toward the ⟨100⟩ directions at 4 monolayers and back again toward the ⟨110⟩ directions at about 8 monolayers. The in-plane spin reorientation that occurs at room temperature is accompanied by significant changes of the magnetic domain structure. In the Frank-van der Merwe growth regime, large magnetic domains are observed in metastable 3 and 4 monolayer films. The isolated three-dimensional Fe islands that form in the Stranski-Krastanov regime have vortex, quasi-single domain (*C* state), or single magnetic domain structures, depending on their size and shape. The detailed results that are obtained with high thickness, lateral and azimuthal angular resolution with spin-polarized low energy electron microscopy are compared with earlier laterally averaging and laterally resolving magnetic studies, and discrepancies are explained.

DOI: 10.1103/PhysRevB.95.064404

I. INTRODUCTION

The study of ferromagnetic thin films and small particles during the last several decades has made major contributions to the understanding of collective magnetic phenomena because of the strong sensitivity of ferromagnetism in these confined structures to dimensionality. Critical behavior, anisotropy, domain structure, and spin reorientation processes are examples of the phenomena that have been studied in this context and are now well understood [1–4]. One of the most interesting ferromagnetic materials is Fe because its magnetic properties are not only very sensitive to its mesoscopic and nanoscopic structure but also to its atomic structure due to the strong dependence of the exchange interaction upon interatomic distance and arrangement: Fe can be nonmagnetic or antiferromagnetic, or it can be collinear or noncollinear ferromagnetic. For this reason it has been the subject of numerous papers, mainly on fcc(001) metals, GaAs(001), W(110), and W(001) surfaces [5–11]. The magnetic properties have usually been probed by measuring a macroscopic response to an applied magnetic field, for example using the magneto-optic Kerr effect (MOKE) or with classical magnetometry, or after applying a magnetic field in remanence by spin-sensitive electron scattering or emission experiments. Investigations at microscopic length scale have also been performed using several spin-resolved microscopies, including scanning electron microscopy with polarization analysis (SEMPA), spin-polarized scanning tunneling microscopy (SP-STM), x-ray magnetic dichroism–photoemission electron microscopy (XMCD-PEEM), and spin-polarized low energy electron microscopy (SPLEEM). The sensitivity of electron beam based methods to a magnetic field, however, limits their use to the study of the virgin state, undisturbed by the application of an applied field, or in remanence after removal of an applied field. Magnetic imaging gives access to important complementary information about domain structure, local magnetization, and the relationship of magnetism to morphology that facilitates a deeper understanding of magnetic phenomena. In particular, the fast image acquisition in SPLEEM allows following the evolution of magnetization during film growth.

In the present paper, we investigated the growth and the structural and magnetic properties of Fe films on the W(001) surface using low energy electron diffraction (LEED), low energy electron microscopy (LEEM), and SPLEEM [12–15]. Investigation of the Fe/W(001) system has a long history, starting from purely structural studies with LEED, Auger electron spectroscopy (AES), work function change ($\Delta\Phi$) measurements, and thermal desorption spectroscopy (TDS) [16–18]. These early studies served as a foundation for combined structural and magnetic studies that were performed later [19–25]. Even more recent work that combined MOKE with STM [26–28] and later employed SP-STM [29,30] brought deeper insight into the structure-magnetism relationship, in

*Present address: School of Physics and Astronomy, Cardiff University, Cardiff, United Kingdom.
†Present address: Femtosecond Spectroscopy Unit, Okinawa Institute of Science and Technology Graduate University, Okinawa, Japan.

particular in films grown at moderately elevated temperatures (∼400−500 K).

Early studies of Fe/W(001) carried out using AES, $\Delta\Phi$, TDS and LEED [16,18] found that a 2 monolayer (ML) pseudomorphic Fe film forms initially during growth at room temperature that is stable up to at least 900 K [18,22]. However, some of the subsequent papers on film growth and stability for studies carried out in connection with magnetic measurements [17,21,23] came to the conclusion that the stable wetting layer was only 1 ML thick. This discrepancy was apparently due to a thickness calibration in the latter work that was based on an erroneous interpretation of AES, TDS, or LEED data. Other early magnetic studies [20,24] perpetuated the same thickness error, which is evident in the temperature or thickness dependence of the magnetic data reported in these papers. Our investigations confirm the reports of a 2 ML thermodynamically stable wetting layer. Therefore, we correct this error as necessary when we refer to the earlier papers [17,20,21,23,24].

Mulhollan *et al.* [20] studied 2–6-ML-thick films grown at room temperature using MOKE and spin- and angle-resolved photoemission and came to the conclusion that the in-plane ⟨110⟩ direction was the easy axis in this thickness range, with coercivities of less than 100 Oe. Chen and Erskine [21] reported coercivities determined using MOKE of about 100 Oe in 3–5-ML-thick films grown at 250 K, independent of direction, but that an extrinsic in-plane uniaxial anisotropy is introduced perpendicular to substrate atomic steps. Jones and Venus [23] made a very detailed study of Fe films grown at room temperature with LEED up to 10 ML, with AES up to 6 ML and by measuring the spin polarization of diffracted electrons up to 8 ML. They concluded that the easy axis was along the ⟨100⟩ direction, based on the low coercivities, ranging from less than 2 Oe at 4 ML to less than 20 Oe at 8 ML. Elmers and Hauschild [22] assumed that the easy axis is aligned with the ⟨100⟩ direction in their detailed study of the temperature dependence of magnetization in 1.2–2.7-ML-thick films using spin-polarized LEED (SPLEED), which showed the onset of magnetism at 300 K at 2.35 ML. Choi *et al.* [24] performed MOKE measurements with magnetic field applied only along the ⟨100⟩ direction in 2.6–4.1-ML-thick films grown at room temperature and also found similar low coercivities (e.g., 17 Oe at 3.4 ML). A comparison of all these earlier magnetic studies does not give a coherent picture of the magnetic properties and easy axis of Fe films on W(001), except that the coercivity and magnetic anisotropy are small.

A much clearer picture emerges from the STM, MOKE, and LEED papers of Wulfhekel *et al.* [26,27], combined with stress measurements of Enders *et al.* [25], which covered larger thickness and growth temperature ranges than earlier papers. To begin with, STM confirmed that small pseudomorphic particles, reported earlier to be either 10 nm [20] or 6 nm [22] in diameter based on LEED, form during the initial growth of nominally 2-ML-thick films at room temperature [27]. With increasing thickness above 4 ML, progressively rougher three-dimensional (3D) growth was observed with STM that also produces diffraction spot broadening and increasing background intensity in LEED [27]. Annealing of thick (rough) room temperature–deposited films to 800 K [27] or to ≈750 K [30] caused the formation of practically fully relaxed 3D crystals on top of a smooth 2-ML-thick wetting layer [27]. At intermediate temperature (i.e., between about 400 and 550 K), growth of fully strained pseudomorphic films occurs up to 4 ML in a quasi-layer-by-layer manner [27]. Above 4 ML, however, depending on growth temperature, two different morphologies are formed. During growth below 500 K, one-dimensionally strained islands elongated along the ⟨100⟩ directions with dislocation bundles along these directions form on the top of 4 ML [26,27]. Between 500 and 550 K, cross-shaped strained crystals grow on the surface through dewetting of the material in excess of 2 ML. In the former below 500 K, one-dimensional strain caused by an approximate 10:9 misfit, visible in LEED in a 9×1 superstructure pattern, is relaxed by dislocations along either of the in-plane ⟨100⟩ directions. The strain relaxation is also clearly visible in stress measurements as a function of film thickness, which shows an initial rapid increase with film thickness in the dislocation-free pseudomorphic film followed by a nearly constant stress between 3.9 and 5.5 ML [25]. Above about 600 K, the growth of compact unstrained 3D crystals was observed directly on top of the 2-ML-thick wetting layer [26,27,29]. Their formation immediately on the wetting layer suppresses the growth of metastable 3 and 4 ML films that was seen between 360 and 550 K.

Detailed information on the magnetic properties of the films was obtained in the MOKE studies by Wulfhekel *et al.* [26,27] and in SP-STM work by von Bergmann *et al.* [29,30]. The MOKE hysteresis loops of films grown at 300 K taken in the ⟨100⟩ and ⟨110⟩ directions were interpreted in terms of a ⟨110⟩ easy axis up to about 6 ML and ⟨100⟩ easy axis at larger thickness. During growth at 400 K, the reorientation transition of the easy axis from ⟨110⟩ to ⟨100⟩ occurred already slightly above 4 ML, coinciding with the formation of dislocations in the elongated islands that grow beyond this point and accompanied by a strong increase of the coercivity, H_c. For example, in films grown at room temperature, H_c only increased from 1.5 Oe at 2.7 ML to 7 Oe at 4.7 ML. In contrast, a 4.3-ML-thick film grown at around 400 K had a substantially higher H_c of 50 Oe**.** The enhanced coercivity obtained at 400 K is also significantly higher than the highest coercivities observed with MOKE in films of any thickness grown at room temperature, which were less than half as large in a 14.2 ML film [27]. The elongated islands and cross-shaped crystals that form at intermediate temperature exhibited complex magnetic structure that depended upon the crystal shapes [26,27,29]. Finally, the domain structure of relaxed 3D crystals prepared by depositing 4.7–6.5 ML Fe at room temperature and annealing at about 800 K was studied also with SP-STM [28]. Both simple vortex and single-domain structures were observed, depending upon crystal width ($\leqslant$200 nm) and height ($\leqslant$20 nm).

Although a large amount of information is already available about the growth of Fe on W(001) and its magnetic properties at a few specific thicknesses, the detailed evolution of magnetism with thickness is not fully understood. SP-STM was used to gain some understanding of how magnetism evolves. However, the crystallographic direction of the magnetic easy axis could not be determined due to instrument limitations. Only a relative 45° rotation between 2 and 3 ML regions and 4 ML regions could be ascertained. Nothing is known about the virgin state in absence of an external magnetic field.

Here we address this gap in our knowledge, using LEEM and SPLEEM [12–15]. In contrast to the earlier postgrowth studies of this system [16–30], growth is monitored continuously with LEEM, and the evolution of the magnetic structure is similarly observed quasicontinuously using SPLEEM in our investigations. The magnetic characterization is performed without applying a magnetic field during measurement. This approach reveals how the virgin magnetic state of Fe films changes with high thickness, lateral and azimuthal angular resolution. Our observations allow the direct correlation of growth morphology, evolving microscopic magnetic domain structure, and macroscopic magnetic properties such as the magnetic easy axis. Interestingly, while some agreement with earlier work is found, we also identify and explain some key discrepancies and clarify some issues on which there has not been agreement in the literature. Finally, our work also provides additional insight about the possible relationship between the magnetism of macroscopic Fe films and 3D crystals on W(001) and the spin polarization of electrons field-emitted from Fe-covered W(001)-oriented tips [31,32].

II. EXPERIMENTAL DETAILS

Experiments were carried out in a conventional LEEM instrument and in a SPLEEM instrument. The imaging principle and contrast mechanisms of LEEM and SPLEEM have been described previously [12–15]. Briefly, LEEM is capable of imaging surfaces in real time using elastically backscattered very low energy electrons. The conventional contrast mechanisms that provide sensitivity to structure and morphology in LEEM are augmented by magnetic contrast in SPLEEM through the use of a spin-polarized electron beam. The magnetic contrast is determined by the exchange asymmetry A_{ex}, which is the difference between the reflected intensities of oppositely polarized incident electron beams divided by the sum of these intensities. A spin polarization manipulator allows orientation of the spin polarization vector of the electron beam in any desired direction with respect to the sample crystallographic directions at arbitrary direction in the sample surface plane, out-of-plane, and in between. The magnetic asymmetry in SPLEEM is proportional to $\boldsymbol{P}\cdot\boldsymbol{M}$, where $\boldsymbol{P}$ is the spin polarization vector of the incident beam and $\boldsymbol{M}$ the local magnetization. In our experiments, the in-plane $\boldsymbol{P}$ direction was referenced to the crystallographic directions of the W(001) surface by assuming that the magnetization easy axes of fully relaxed compact 3D islands grown at temperatures above 700 K are along the ⟨100⟩ directions, as in bulk Fe, and that the Fe islands grow with edges parallel to these low index substrate directions. Moreover, the cross-shaped structures grown at 500 K are known from earlier studies to be magnetized in the direction of their long axes, which are parallel to the ⟨100⟩ directions [26,27]. Using these two criteria, the orientations of $\boldsymbol{P}$ with respect to $\boldsymbol{M}$ that produced the maxima of the asymmetry in azimuthal plots correspond to the ⟨100⟩ directions of W(001). These directions are identified in our notation by the beam polarization azimuthal angles $\phi = 0^\circ$, 90°, 180°, and 270°.

For the relatively large fields of view imaged in this work, the spatial resolution was limited not by the electron optical properties of the instrument, but by the image pixel size relative to the fields of view to 15 nm in LEEM and 50 nm in SPLEEM. Furthermore, the quoted resolution of SPLEEM in the magnetic imaging mode included an estimated contribution of image drift that occurred during image integration. The low signal-to-noise ratio that necessitated image integration was mainly due to the relatively low spin polarization of the imaging electron beam, which is about 20% in this study. SPLEEM magnetic images of the most well-defined magnetic domains (e.g., see Fig. 8 below) provide some insight about the angular resolution of the magnetic measurement. The full-width half-maximum (FWHM) of the sharpest sample magnetization direction distributions (with bin size of 1°) were about 3°. Considering that the FWHM may also be contributed to by nonuniformity of the magnetization direction itself, this quoted angular resolution has to be considered to be an upper limit of the instrumental value. Furthermore, magnetization directions present in domains that can be expected to be along orthogonal in-plane ⟨100⟩ directions, in principle, were determined experimentally to be within 1.5° or less of being orthogonal and aligned with the expected in-plane directions. This confirms the high angular resolution of the SPLEEM magnetic measurements, as well as the absolute correctness of the detected magnetization directions.

The base pressure in the two microscopes was in the low 10^{-10} Torr regime. The W(001) sample was oriented to within 0.1° of the [001] direction. It was cleaned by annealing at 1200–1400 K in an oxygen pressure of 1×10^{-7} to 1×10^{-6} Torr and flashing to above 2000 K. Fe was deposited reproducibly from an electron beam–heated source in the LEEM or a resistively heated source in the SPLEEM. The pressure increased to about 5×10^{-10} Torr during Fe deposition. The deposition rate was determined by the periodic intensity oscillations of LEEM images during Fe deposition at 600 K, as reported below. Deposition rates from 0.10 to 0.20 pseudomorphic ML/min were used. Deposition temperatures ranged from 300 to 800 K and were measured with a W/Re3%−W/Re25% thermocouple spot-welded to the support ring on which the crystal was pressed firmly by a cap. In this temperature range, precise temperature measurement is notoriously difficult because of temperature gradients between the crystal center and thermocouple, which depend on heating mode and mounting. Therefore, significant differences between different instruments are not unusual.

III. EXPERIMENTAL RESULTS

A. Growth

The growth of Fe on W(001) at various temperatures is illustrated in Fig. 1 by the variation of LEEM image intensity, integrated over a 6 μm field of view, as a function of thickness in pseudomorphic MLs. The data in Fig. 1 are taken from LEEM movies of film growth at each temperature (see Supplemental Material for LEEM movies of film growth at 400–700 K [33]). The film thickness in Fig. 1 is calibrated by the deposition time to reach the intensity maxima at the highest temperatures at which surface mobility is high enough for the first two monolayers to grow nearly perfectly layer by layer. The intensity oscillations that are observed at all temperatures initially occur because the nucleation of small islands on the bare substrate and on top of the completed first and second layer introduces steps that scatter reflected

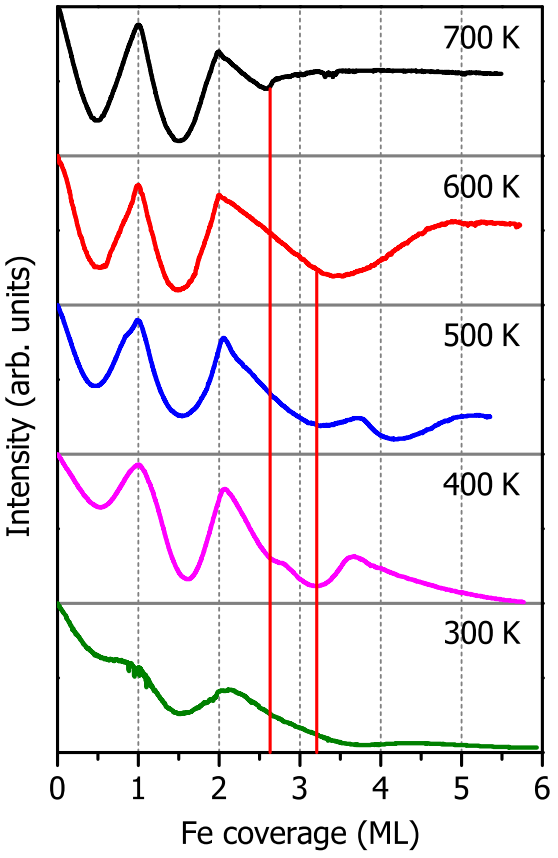

FIG. 1. LEEM image intensity oscillations during deposition of Fe on the W(001) surface at several deposition temperatures. The thickness scale is in pseudomorphic MLs. The red vertical lines indicate 2.63 and 3.21 ML, respectively. See the text for the discussion about these thicknesses. The imaging electron energy is 9.0 eV.

electrons outside the angle-limiting contrast aperture. The increasing diffuse scattering that occurs during further island nucleation and growth reduces the image intensity until the point that the step density is at its highest before islands begin to coalescence significantly, corresponding to the intensity minima seen at about half integer layer thickness. The diffuse scattering diminishes with the reduction of the step density, and the integrated image intensity increases from that point until the layer is completed. Selected frames of the 600 K growth movie are shown in Fig. 2 that demonstrate how the layer-by-layer growth morphology correlates with the initial intensity changes presented in Fig. 1: in Figs. 2(a) and 2(c), smooth terraces are observed between atomic steps on the bare surface and between the replicated steps on the complete Fe monolayers, whereas in Fig. 2(b), the intensity is strongly reduced due to diffuse scattering from numerous unresolvable islands at half-integer film thickness, and in Fig. 2(d), small islands can be seen at a small excess above a complete layer.

At lower temperatures, the mobility of the Fe atoms is so low that second and third monolayer islands already form before the first and second monolayers are completed, respectively. This shifts the intensity maxima in Fig. 1 to higher average thickness and reduces their sharpness, as is particularly evident at 300 K. In deposition at this temperature, the first broad intensity peak is located near the 1 ML position, and

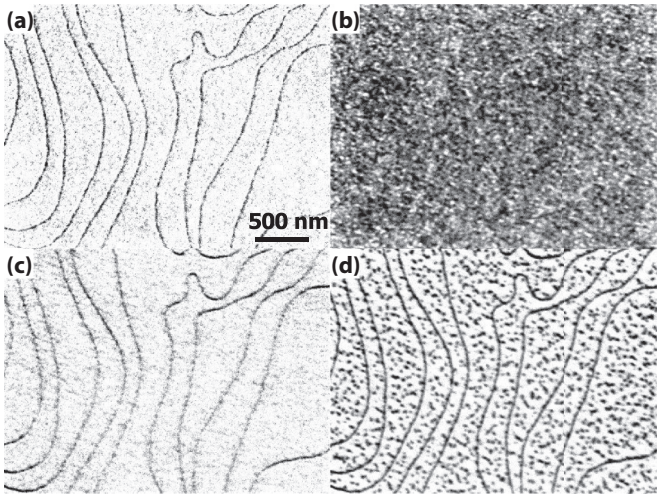

FIG. 2. LEEM video frames from the early stages of Fe growth on W(001) at 600 K. (a) Clean surface, (b) 1.5 ML, (c) 2 ML, (d) 2.2 ML. The imaging energy is 9.0 eV.

the similarly broadened second maximum can be discerned at 2.13 ML. Rough film growth at 300 K produces no discernible features in LEEM images. In the 400 K deposition, the sharper peak at the 1 ML position and the slightly delayed and similarly sharper second maximum at 2.07 ML are followed by a minimum at 3.23 ML and a maximum at 3.65 ML. These latter two features can be identified in the LEEM images as being caused by high and low particle densities, respectively, which are present during the simultaneous growth of the third and fourth monolayers. The peak at 3.65 ML signals the delayed nominal completion of the third layer. Beyond this peak, the roughness increases continuously, although the fine structure of this roughness is below the resolution limit of the measurement in the present study.

At higher deposition temperatures, significant morphological changes occur above 2 ML that are most pronounced at 700 K. At 700 K, the intensity decreases linearly beyond 2 ML until a small but sudden increase begins at 2.63 ML. LEEM shows that 3D crystals nucleate at this coverage and grow very rapidly (see Supplemental Material for LEEM Movie S1 of film growth at 700 K [33]). Three-dimensional crystals are shown after deposition of 2.95 ML at 700 K in Fig. 3(a). The linear decrease of the intensity beyond 2 ML is attributed to either of two possible causes. It may occur due to the presence of a two-dimensional (2D) gas of Fe adatoms that scatters electrons diffusely. The diffuse scattering increases and the intensity

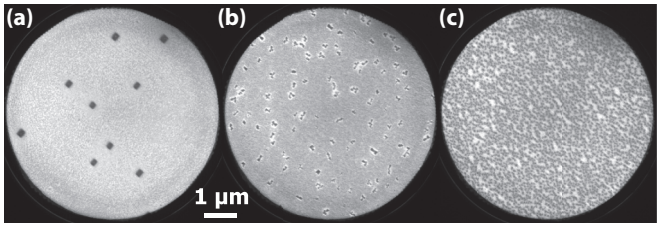

FIG. 3. LEEM video frames of the film morphology after nucleation of 3D Fe crystals on W(001) at several deposition temperatures. (a) 700 K, 2.95 ML, (b) 600 K, 3.63 ML, (c) 500 K, 4.0 ML.

decreases with increasing gas density during deposition until 3D islands nucleate. A mild reduction of the supersaturated 2D adatom gas density that occurs when 3D crystals nucleate will diminish the diffuse scattering. This can account for the sudden small intensity rise that follows the linear decrease. Alternatively, the decreasing intensity may be caused by the partial growth of the third layer. Correspondingly, the small intensity rise upon 3D crystal nucleation will be caused by dewetting of the condensed third monolayer that exposes the brighter 2 ML film below. The 3D crystals that form at this temperature are dark because they are bounded on top by facets, whose reflected beams are intercepted by the contrast aperture. The facet orientation was determined from the movement of the facet spots in the LEED pattern as a function of energy [34]. A plot of the perpendicular vs parallel momentum transfer of the facet spots in the azimuth of their movement clearly shows that the facets are {310} planes. According to first principles theory calculations [35], this orientation has slightly higher surface energy than the other low energy faces {211}, {111}, {100}, and {110}.

During growth at 600 K, the intensity also decreases linearly above 2 ML, but now over a broader coverage range that extends up to 3.36 ML. The initial decrease is not due to a 2D gas but, as LEEM clearly shows, to the simultaneous growth of third and fourth layer islands, which differ slightly in brightness, on top of the complete 2 ML film (see Supplemental Material for LEEM Movie S3 of film growth at 600 K [33]). The nucleation of 3D crystals begins already at 3.21 ML. It triggers the simultaneous dewetting of the surrounding third and fourth layers, and the crystals continue to grow on top of the exposed double layer during dewetting. These abrupt changes in the growth mode do not change the initial linear intensity decrease because the effect of the growing dark crystals on the average intensity is compensated for by the expanding bright 2 ML regions surrounding them. Figure 3(b) shows the surface after about 0.4 ML has been deposited beyond the nucleation coverage (see Supplemental Material for detailed analysis of the nucleation and growth process [33]). The crystals are initially mostly elongated along the ⟨100⟩ directions. With increasing thickness there is a transition from elongated crystals to thicker 3D, more isometric crystals, which preferentially form at the ends of the initial linear structures [Fig. 4(a)].

Growth beyond 2 ML at 500 K apparently also occurs by single- and double-layer islands. However, shortly before the 4 ML film is completed, 3D crystals nucleate at 3.72 ML and grow rapidly in number with further deposition (see Supplemental Material for LEEM Movie S4 of film growth at 600 K [33]). Intensity differences between 2, 3, and 4 ML regions allow 2 ML rims surrounding 3D crystals to be detected initially that are themselves separated by 3 and 4 ML regions [Fig. 3(c)]. With increasing deposition, not only do the 3D crystals grow in size and somewhat in number, but the 2 ML rims also gradually expand, leaving fewer and fewer 3 and 4 ML regions between them. Obviously, the third and fourth layers are also not stable at 500 K. However, due to the limited LEEM resolution, it is difficult to distinguish the detailed morphology of the 3D crystals.

The film growth just described was carried out in the LEEM system. However, a film grown in the SPLEEM system supposedly at the same temperature, 500 K, as in Fig. 3(c) showed a quite different morphological evolution with thickness. For example, the film morphology that forms during growth in the SPLEEM at 500 K in Fig. 4(b) clearly differs from the small 3D crystals observed during growth at this temperature in the LEEM [Fig. 3(c)]. Instead, the morphology observed in the SPLEEM at 500 K [Fig. 4(b)] is similar to what was observed previously in STM studies after growth of about 4.7 ML, also at about 500 K [27]. This morphology is also observed in the LEEM but at a temperature below 500 K. Therefore, we conclude on the basis of the temperature-dependent film morphology that the temperatures determined in the SPLEEM and reported in earlier STM studies in Ref. [27] are comparable, but that both are overestimates relative to the temperature determined in LEEM. Furthermore, morphologies observed at lower temperature, ∼400 K, in Ref. [27] were formed at 500 K in other STM work [29]. These discrepancies show that the temperatures reported in this paper and earlier papers [27,29] have to be taken with a grain of salt because of the inherent difficulty of measuring temperature with absolute accuracy and reproducibility in different vacuum systems.

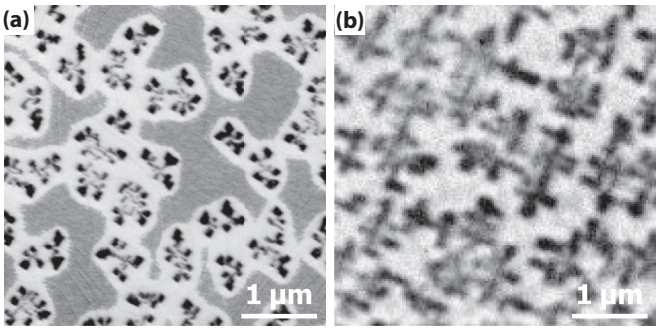

FIG. 4. LEEM video frames showing (a) 3D crystals at 600 K, 6.0 ML (in LEEM) and (b) quasi-2D elongated crystals at 500 K, 5.0 ML (in SPLEEM). In (a) 3 ML (dark gray) and 2 ML (light gray) regions are present between crystals (black). Note that panel (a) was taken from a different experiment than that shown in Fig. 3(b). The imaging electron energy is (a) 9.0 eV and (b) 0.5 eV.

B. Magnetism

The evolution of magnetic domain structure was studied during film growth at room temperature and after cooldown to room temperature following film growth at elevated temperature. Fast acquisition of quasi-real-time SPLEEM movies during continuous growth at room temperature necessitated the use of a fixed incident beam polarization direction. This constraint limits information obtained to the magnetization component along one in-plane direction (i.e., an in-plane ⟨100⟩ direction in our work) (see Supplemental Material for SPLEEM Movie S6 [33]). The thickness resolution under these quasi-real-time growth conditions was 0.009 ML, determined from the deposition rate, 0.11 ML/min, and magnetic image acquisition interval. Consistent but more detailed information about the magnitude of the asymmetry signal and azimuthal orientation of the magnetization is obtained from pairs of SPLEEM images that were obtained with $\boldsymbol{P}$ along two orthogonal ⟨100⟩ and ⟨110⟩ directions during a "cumulative"

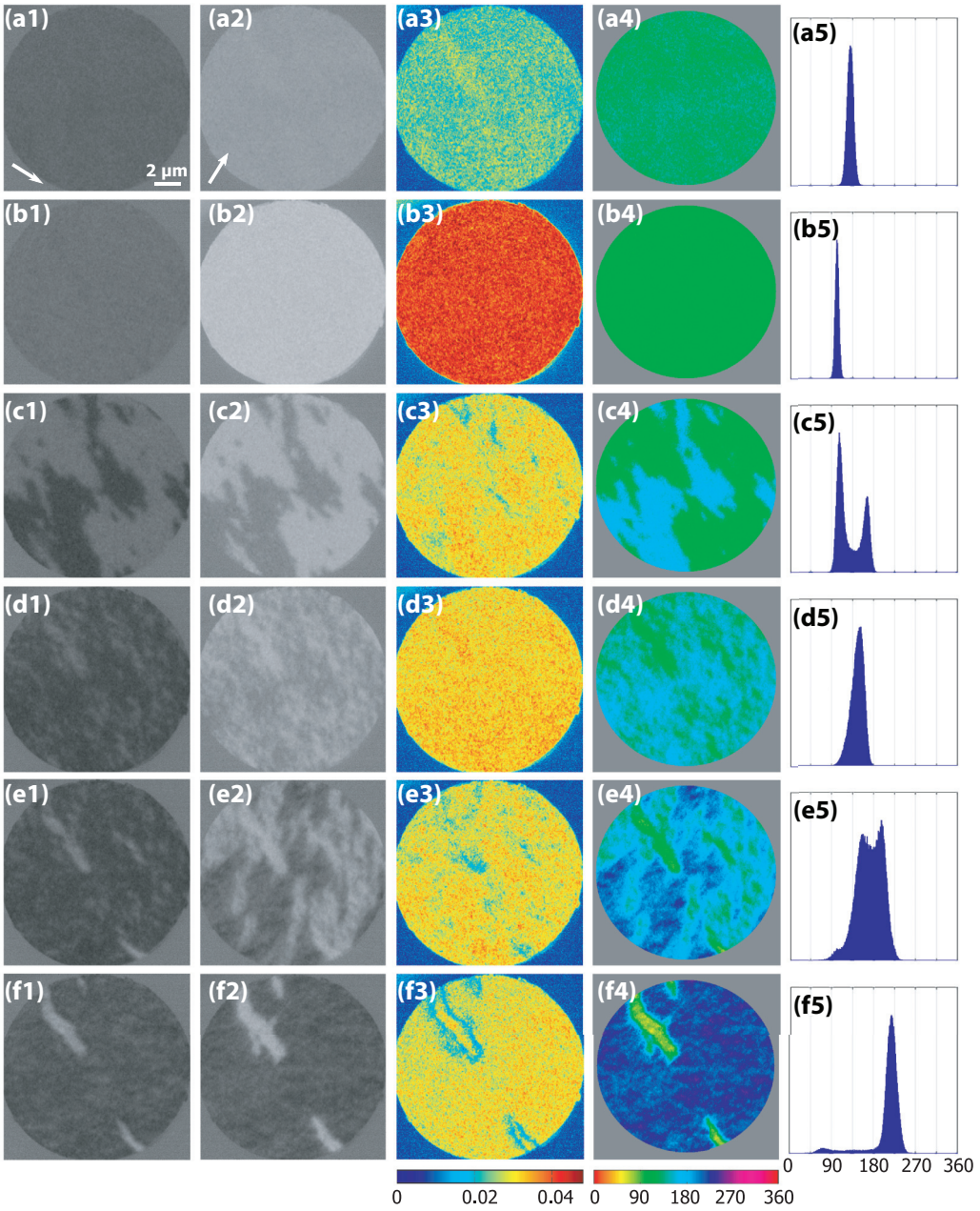

FIG. 5. Selected SPLEEM images taken during growth of Fe on W(001) at room temperature: (a) 2.98, (b) 3.76, (c) 5.01, (d) 6.66, (e) 7.36, (f) 8.62 ML. The figure shows from left to right: image taken with polarization (1) parallel to [100] direction, (2) parallel to [010] direction, as arrows point, respectively; composite images that present (3) magnitude of the magnetic asymmetry and (4) magnetization direction; and (5) histogram of the angular distribution of the magnetization direction calculated pixel by pixel from (4). The imaging electron energy is 0.5 eV. See Supplemental Material for a full set of results [33].

deposition sequence. In the cumulative sequence, deposition was interrupted at 0.16 ML intervals for a short time to record the two orthogonal SPLEEM image pairs before restarting growth. A selection of SPLEEM images obtained at different film thickness in this way is shown in Fig. 5 (see Supplemental Material for a full set of results [33]). For each thickness [Figs. 5(a)–5(f)], Figs. 5(1) and 5(2) show the SPLEEM images with $\boldsymbol{P}$ along the [100] and the [010] substrate directions, respectively, Figs. 5(3) show the magnetic asymmetry magnitude evaluated from Figs. 5(1) and 5(2) at single-pixel resolution independent of $\boldsymbol{M}$ direction, Figs. 5(4) show the $\boldsymbol{M}$ direction evaluated from Figs. 5(1) and 5(2) at pixel resolution independent of magnetic asymmetry magnitude, and Figs. 5(5) show the histogram of the $\boldsymbol{M}$ directions present in Figs. 5(4). Calculation of the vector sum over the full fields of view of the two composite color images Figs. 5(3) and 5(4) at every film thickness gives the average magnetic asymmetry magnitude and a representation of the $\boldsymbol{M}$ direction distribution as functions of Fe film thickness that are shown in Fig. 6. More detailed information that was extracted from the composite images of Figs. 5(3) and 5(4) at every thickness by pixel-by-pixel analysis is also compiled in Fig. 7(a) for

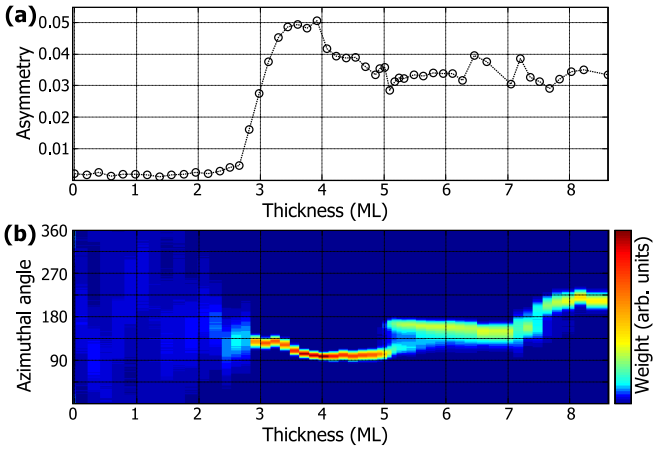

FIG. 6. (a) Magnitude of the magnetic asymmetry and (b) angular distribution of the magnetization direction averaged over the field of view of the SPLEEM images obtained during Fe film growth at room temperature (Fig. 5, and see Supplemental Material [33]), with $\phi = 0°$, 90°, 180°, and 270° corresponding to in-plane ⟨100⟩ directions. The color code in panel (b) represents the pixel number at each angle relative to the maximum value (dark red) of the whole angular distribution.

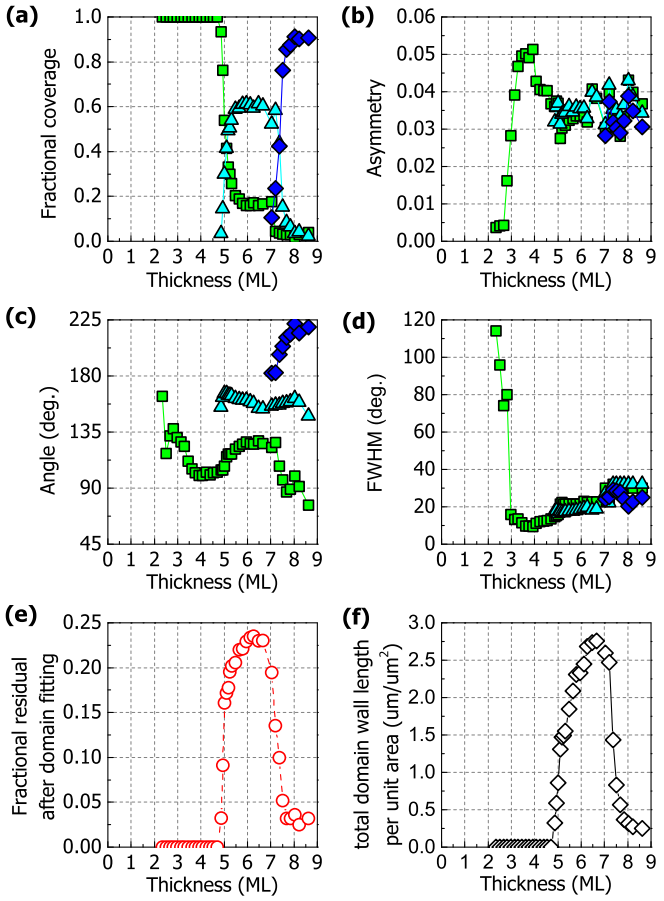

FIG. 7. Local (pixel-by-pixel) data derived from the SPLEEM images obtained during Fe film growth at room temperature (Fig. 5, and see Supplemental Material [33]). The properties of the three domain orientations (green, cyan, blue), which dominate at different coverages, are (a) fractional coverage, (b) magnetic asymmetry, (c) magnetization direction, (d) FWHM of the angular distribution of the magnetization direction, (e) fractional residue after domain fitting, and (f) total domain wall length per unit area.

the fractional coverage f_d and Fig. 7(b) for the exchange asymmetry $A_{ex,d}$ of the different domains resolved in SPLEEM images, Fig. 7(c) for the azimuthal angle of $\boldsymbol{M}$ with respect to the [100] direction ($\phi = 0$) within the domains, Fig. 7(d) for the FWHM of the angular distribution of $\boldsymbol{M}$ within each domain, Fig. 7(e) for the fractional coverage residue f_r left afer fitting the domains, and Fig. 7(f) for the total domain wall length per unit area (see Supplemental Material for details on the fitting procedure and results [33]).

A weak magnetic signal appears already at 2.35 ML, although with broad angular distribution, during cumulative growth at room temperature [Figs. 6(b) and 7(a)–7(d)]. The magnetic asymmetry signal increases with thickness rapidly, simultaneously as the angular distribution narrows strongly close to the [$\bar{1}$10] direction [Fig. 6, and green squares in Figs. 7(b)–7(d)]. The magnetization direction is sharply aligned very near to the [$\bar{1}$10] direction ($\phi = 135°$) at about 3.0 ML [Figs. 5(a), 7(c), and 7(d)], and the asymmetry magnitude reaches a maximum value at about 3.5 ML [Fig. 7(b)]. With further increasing thickness, $\boldsymbol{M}$ rotates towards the [010] direction ($\phi = 90°$), though not completely [Figs. 6(b) and 7(b)]. Simultaneously, the angular distribution decreases modestly and reaches a minimum FWHM at about 4 ML [Fig. 7(d)]. Above 4.7 ML, new domains develop, with $\boldsymbol{M}$ oriented initially more than 45° away from the original single domain state [Figs. 5(c) and 6(b), and cyan triangles in Fig. 7] and grow rapidly, resulting in equal coverage of the two domains at 5.1 ML [Fig. 7(a)]. With further increasing thickness, the coverage of the original domains continues to decrease as they also break up further into smaller sized domains. This results in a maximum of the domain wall density at 6.66 ML [Figs. 5(d) and 7(f)]. At about 7 ML, a new domain suddenly appears with $\boldsymbol{M}$ approximately orientated in the [$\bar{1}$00] direction ($\phi = 180°$) [blue diamonds in Figs. 7(a)–7(d)]. This domain grows rapidly with further increasing thickness [Fig. 7(a)], with $\boldsymbol{M}$ rotating continuously away from the [$\bar{1}$00] [Fig. 7(c)] and into the [$\bar{1}$ $\bar{1}$0] direction ($\phi = 225°$) at the largest thicknesses [Figs. 6(b) and 7(c)]. An intermediate state of this rotation at 7.36 ML is shown in Figs. 5(e). Above 8 ML, this domain is dominating, and only remnants of the two domains observed at lower thickness remain [Figs. 5(f) and 7(a)]. Changes in the domain wall density [Fig. 7(f)] are connected with the micromagnetic changes. They are accompanied by corresponding variations of the fractional coverage residue f_r [Fig. 7(e)] due to the strong serration of the domain walls and the resulting difficulty in fitting the domain boundaries.

Growth at 400 K differs significantly from that at room temperature, as seen in Fig. 1. The effect upon magnetism is shown in Fig. 8 for films deposited continuously to different integer layer thicknesses. At 3 ML, there is a multidomain state, with $\boldsymbol{M}$ preferentially in any of the ⟨100⟩ directions, with considerable angular spread and possibly a small admixture of ⟨110⟩$\boldsymbol{M}$ directions, as seen in the histogram [Figs. 8(a)]. This contrasts sharply with the single domain state with $\boldsymbol{M}$ narrowly pointing along a [110] direction that was observed

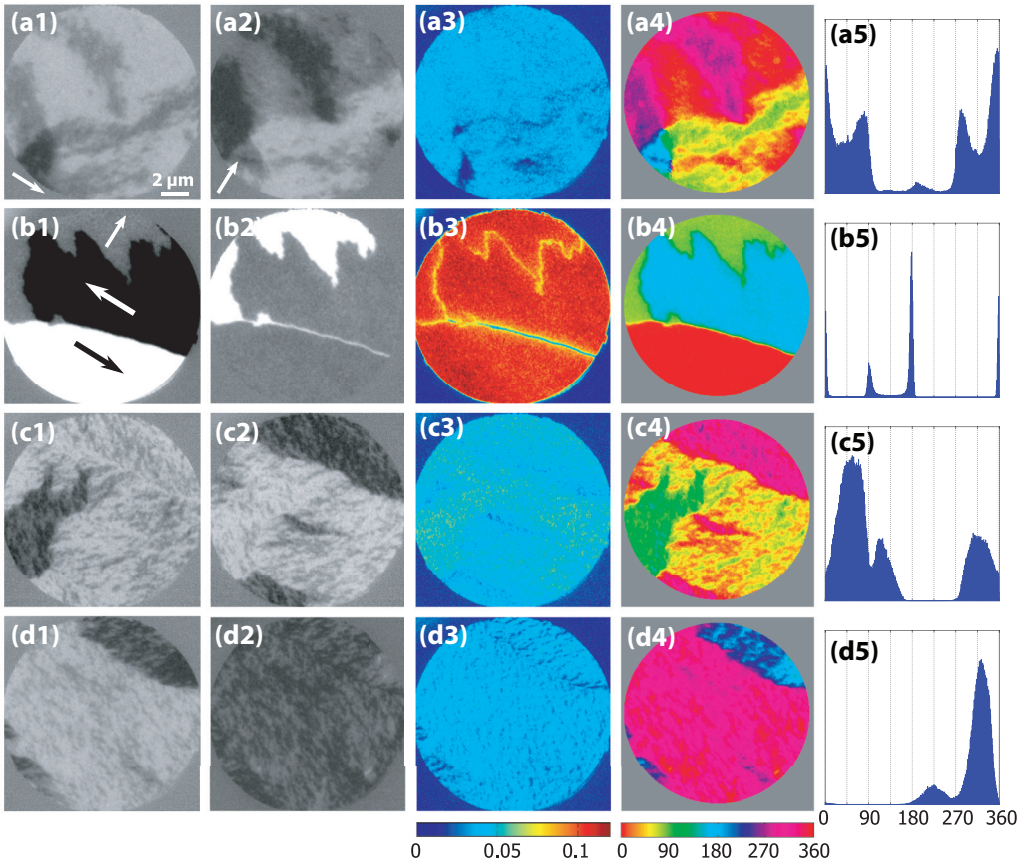

FIG. 8. SPLEEM images of films grown at 400 K, measured at room temperature: (a) 3 ML, (b) 4 ML, (c) 5 ML, and (d) 6 ML. The figure shows from left to right, image taken with polarization (1) parallel to [100], (2) parallel to [010], composite images that present (3) magnitude of the magnetic asymmetry and (4) magnetization direction and (5) the histogram of the angular distribution of the magnetization direction calculated pixel by pixel from (4). The arrows in the top row indicate the [100] and [010] directions, respectively, the arrows in the second row indicate the magnetization directions in the domains. The imaging electron energy is 0.5 eV.

in 3 ML films during growth at room temperature [Figs. 5(b), 6(b), 7(a), 7(c), and 7(d)]. In 4 ML films grown at 400 K, the angular spread has narrowed very strongly around the ⟨100⟩ directions precisely, resulting in large domains [Figs. 8(b)]. This is similar to 4 ML films grown at room temperature [Figs. 5(c)], except for their small misalignment of $\boldsymbol{M}$ from ⟨100⟩. A pronounced ripple domain structure is detected in 5 and 6 ML films grown at 400 K [Figs. 8(c) and 8(d)] that is also somewhat noticeable in films in this thickness range grown at room temperature [Figs. 5(c)]. The $\boldsymbol{M}$ direction also exhibits a wide angular distribution following preparation of 5 and 6 ML films at 400 K that is now clearly around the ⟨110⟩ directions. The distribution narrows somewhat from 5 to 6 ML. Thus, above 4 ML a strong change in the forces that determine the $\boldsymbol{M}$ direction occurs. No fractional ML thicknesses were studied, so the $\boldsymbol{M}$ direction at the onset of magnetic order below 3 ML and the transition between the various $\boldsymbol{M}$ orientations and angular distributions observed at larger integer layer thickness in films prepared at 400 K shown in Fig. 8 are not known.

The magnetic domain structure of films grown at intermediate temperatures was studied only in films grown at 600 K at a few discrete thicknesses. The domain evolution at 500 K is expected to be similar to that at 600 K because of the similarity of growth at 500 and 600 K that was observed in LEEM movies. As noted above, the key differences between the growth at these two temperatures are that the nucleation of 3D crystals is delayed from 3.21 ML at 600 K to 3.72 ML at 500 K and that the 3D crystals form with higher density and smaller size at 500 K due to kinetic limitations. An example of a film grown by deposition of 5.8 ML Fe at 600 K is shown in Fig. 9. At this temperture and coverage, the metastable film that forms initially is partially dewetted following 3D crystal nucleation. The morphology comprises the 2-ML-thick nonmagnetic wetting layer and the 3- and 4-ML-thick regions and clusters of small, interconnected 3D crystals. Figure 9(a) shows the LEEM image, Figs. 9(b) and 9(c) show the SPLEEM images taken with $\boldsymbol{P}$ along the [100] and [010] directions, respectively, and Fig. 9(d) shows the magnitude of the asymmetry A_{ex} determined at pixel resolution from Figs. 9(b) and 9(c). In the bottom row, the angular $\boldsymbol{M}$ distribution is displayed in Fig. 9(e) for 3-ML-thick regions and in Fig. 9(f) for 4-ML-thick regions, while Fig. 9(g) illustrates the complex $\boldsymbol{M}$ distribution on the interconnected 3D crystals. Finally, Fig. 9(h) shows the histograms of the $\boldsymbol{M}$ distributions derived from Figs. 9(e) and 9(f). The domain structure represented in the images and histograms of the 3 and 4 ML regions in Figs. 9(e), 9(f), and 9(h) agree well with those that are present in the continuous films grown at 400 K that are

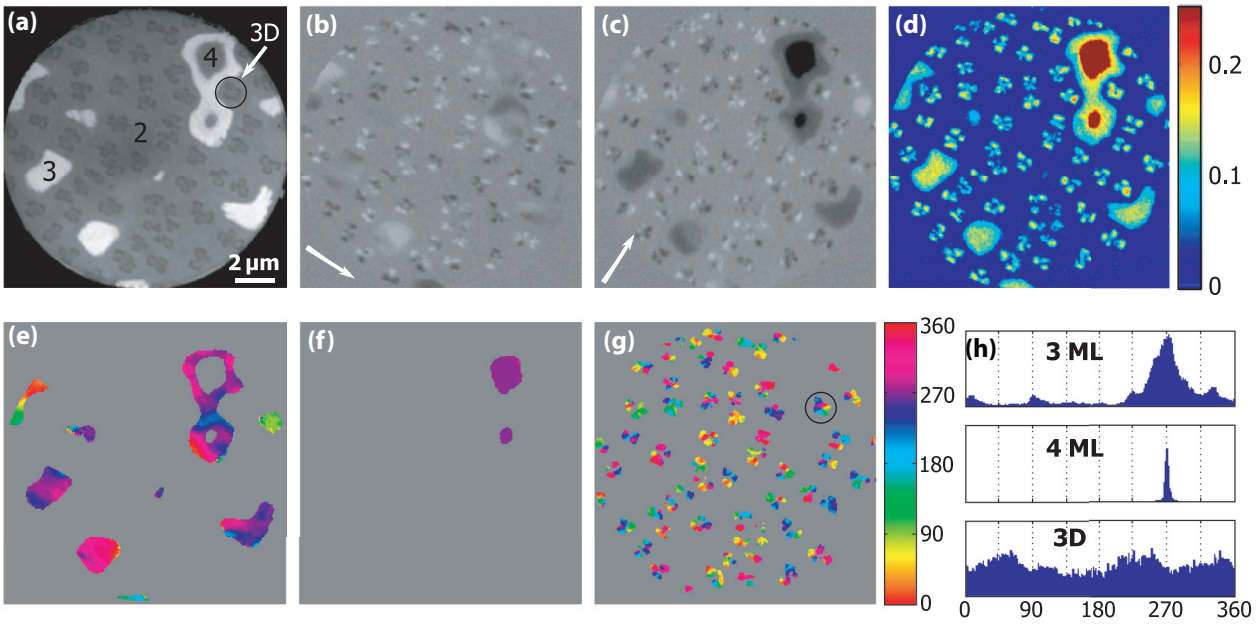

FIG. 9. (a) LEEM and (b, c) SPLEEM images with the polarization parallel to [100] and [010], respectively, of a 5.8-ML-thick Fe film grown on W(001) at 600 K, measured at room temperature. The (d) composite image of images (b) and (c) shows the magnitude of the magnetic asymmetry. The angular distribution of the magnetization direction in 3- and 4-ML-thick regions are shown in panels (e) and (f); that in the 3D crystals is shown in panel (g). (h) Pixel-by-pixel analysis of these images gives the angular magnetization distribution histograms. The imaging electron energy is 0.5 eV.

shown in Fig. 8: a broad angular $\boldsymbol{M}$ distribution preferentially around the ⟨100⟩ directions at 3 ML and large domains at 4 ML with $\boldsymbol{M}$ sharply confined to one of the in-plane ⟨100⟩ directions. The magnetization of the 3D crystals in Figs. 9(g) and 9(h) cannot be compared with that of the continuous 5- and 6-ML-thick films in Fig. 9 because the average thickness of the crystals is much larger than the 5.8 ML that was deposited in Fig. 9. It is nevertheless interesting that the magnetization of the crystals is not aligned along the ⟨100⟩ directions but is nearly isotropic on average. This is a consequence of the nearly random connections between the crystals in the clusters seen in Figs. 9(a) and 9(g) that form during dewetting [see also Fig. 4(a)]. The $\boldsymbol{M}$ direction in each cluster is then determined to a large extent by the shape of the cluster and the degree of contact between the crystals in the cluster. For example, an isolated nearly square cluster, marked by circles in Figs. 9(a) and 9(g), shows predominantly a vortex structure with all in-plane magnetization orientations present.

As already discussed in Sec. III A, Fe forms isolated 3D crystals directly on the 2 ML wetting layer during growth at even higher temperature, 700 K. Due to the high mobility of Fe at this temperature, the crystals have a simple square or rectangular shape with consequently simple magnetic domain structures. This is illustrated in Fig. 10 for a deposition of nominally 5 ML Fe at about 700 K. The top row shows [Fig. 10(a)] a LEEM image and two SPLEEM images taken with $\boldsymbol{P}$ along [Fig. 10(b)] the [100] and [Fig. 10(c)] the [010] directions. High magnification images of selected crystals marked in the top images are shown in the second, third, and fourth rows: LEEM [Figs. 10(d), 10(h), and 10(l)], SPLEEM with $\boldsymbol{P}$ along the [100] [Figs. 10(e), 10(i), and 10(m)] and [010] directions [Figs. 10(f), 10(j), and 10(n)]. From these images the domain structures shown in the last column [Figs. 10(g), 10(k), and 10(o)] can be derived. The average island height is estimated to be 13.4 nm from the total island area, the amount of deposited Fe (5 ML) taking into account the area of the 2 ML wetting layer between islands but not taking into account the shallow {310} faces on the top of the 3D islands.

IV. DISCUSSION

The results presented in Sec. III and in the Supplemental Material [33] show the complexity of the growth and evolution of the spontaneous magnetization and magnetic domain structure of Fe films on W(001). These results will now be discussed and compared with previous results for this system and for Fe films on some other W substrates. This discussion is divided into two parts that focus on films grown at room temperature and films grown at elevated temperatures and subsequently measured at room temperature, respectively.

A. Room temperature growth

The intensity of the (00) diffraction beam vs time during growth at 300 K (Fig. 1) and the LEEM movie from which it was taken provide evidence that the growth of the second and third layers occur with high 2D island nucleation density before the growth of the first and second layers, respectively, are completed. In fact, the STM observation of an ∼2 ML thick film [27] shows that 3-ML-thick islands with an average size near the superparamagnetic limit have already formed while the second layer is still far from being completed. This is close to the thickness, ∼2.35 ML, determined by SPLEED and MOKE that has a Curie temperature of $T_C = 300$ K [22,27].

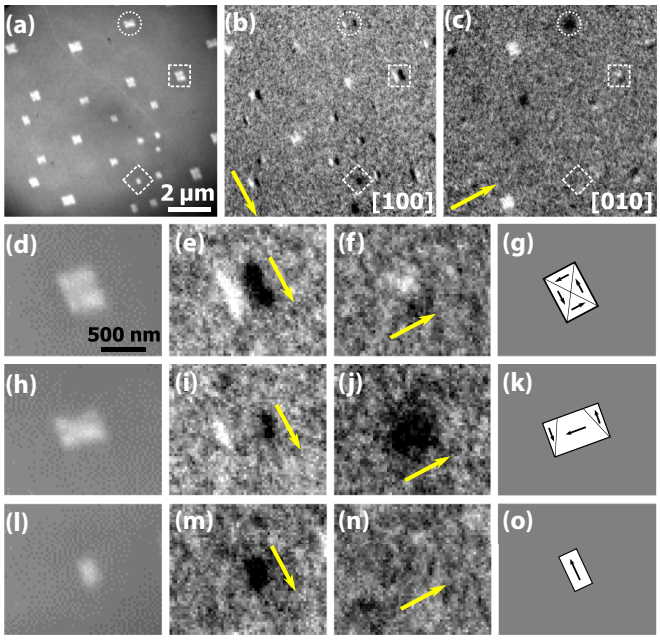

FIG. 10. (a) LEEM and (b, c) SPLEEM images of a 5-ML-thick film grown at about 700 K, measured at room temperature. The polarization direction in panels (b) and (c) is parallel to [100] and [010], respectively. The following rows show the corresponding magnified images of individual crystals and their interpretation: (d–g) a large square crystal, (h–k) a large rectangular crystal, and (l–o) a small rectangular crystal with vortex, *C*-state, and single domain structure, respectively.

Magnetic signal should be detected in our experiments when the nominal film thickness exceeds this critical thickness. However, the film morphology at and after the magnetic onset at 300 K still consists of separate small islands up to 3 ML in height, as seen in STM [27]. Therefore, the magnetization direction varies considerably across the film, as seen in our work in Figs. 7(c) and 7(d), while the Curie temperature still remains relatively close to the growth temperature after the onset thickness. We find that the magnetization becomes more well defined and attains a narrow angular distribution close to the $[\bar{1}10]$ direction only after deposition of three monolayers. This initial well-defined orientation is consistent with the most recent MOKE results [26,27].

With further increase of the film thickness, the roughness increases, as was clearly seen with STM [27]. The kinetic roughening of the film also causes the continuous decrease of the (00) diffraction intensity (Fig. 1). Simultaneously, we observe that the magnetization direction rotates from the $[\bar{1}10]$ towards the [010] direction [Figs. 6(b) and 7(c)], the angular spread of the magnetization further decreases slightly [Fig. 7(d)], and the magnitude of asymmetry increases [Fig. 7(b)], reaching extremal values of 8° off [010], 9° FWHM, and $A_{ex} = 0.052$, respectively, at 3.9 ML. While SPLEEM images appear to show a single domain during the evolution of magnetization in this thickness range, slightly mutually misaligned domains are seen under close inspection in the SPLEEM movie acquired with $\boldsymbol{P}$ along the [100] direction, particularly between 3.3 and 3.7 ML (see Supplemental Material for detailed SPLEEM image analysis and SPLEEM Movie S6 [33]). Thus, the [100] easy axis in the virgin state is actually not very well defined. This may explain the low magnetic anisotropy that was deduced from hysteresis curves in earlier papers [21,23]. It should be noted that the angular distributions shown in Fig. 7(d) were obtained pixel by pixel. We found that the use of n × n pixel binning in the anlysis leads to a decrease of the FWHM approximately proportional to $\sqrt{n}$. This behavior indicates that the measurement is limited by noise. This is understandable because the low spin polarization of the incident electron beam gives a spin-dependent magnetic contribution to the total reflected signal that is small compared with the large spin-independent nonmagnetic contribution. Consequently, the signal-to-noise ratio in the asymmetry, which is the small difference between large signals, is very small. Taking this into account, it is likely that the film really only reaches the true single domain state at 3.9 ML thickness.

Up to this thickness, 3.9 ML, at which the Fe film approaches and apparently reaches a single domain state, the evolution of the magnetization direction with thickness revealed by SPLEEM is notably more complex than detected in earlier studies. This behavior cannot be explained simplistically in terms of bulklike anisotropy and brings into question earlier interpretations. In this thickness range, film growth is known from earlier work to be accompanied by a rapid increase of tensile stress, attributed to epitaxial strain [25]. This strain is huge because of the 10% lattice mismatch between Fe and W. This may affect the magnetic anisotropy and magnetic easy axis via magnetostrictive effects that couple with anisotropic elastic properties of the the Fe film [26,27]. The dilation of the Fe lattice parallel to the surface also has to be coupled with a vertical relaxation to conserve the atomic volume. This gives a lattice constant of 2.351 Å normal to the surface, corresponding to a c/a ratio of 0.82. For such a large tetragonal distortion, easy axis considerations applicable to bulk Fe are certainly not valid. Furthermore, shape anisotropy effects associated with a possible anisotropic island morphology and coalescence may also come into play and influence the easy axis during film growth. The influences of the various effects mentioned here may account for the complex behavior that is revealed by SPLEEM.

Between about 3.9 and 4.9 ML, the fourth monolayer fills up and 5-ML-thick islands grow increasingly. The direction of the magnetization and its angular distribution are observed here to be nearly constant in this thickness range. This is also the thickness range in which constant stress was observed in earlier studies of the growth at 300 K, which was attributed to partial stress relaxation due to the introduction of misfit dislocations [25]. In STM studies of films grown at 400 K, misfit dislocations running along ⟨100⟩ directions actually have been observed in quasi-2D crystals, elongated along the ⟨100⟩ directions on top of dislocation-free 4-ML-thick regions. They were held responsible for introducing a ⟨100⟩ easy axis at 400 K [26,27]. However, it is unlikely that the same phenomena can occur at 300 K for two reasons: (i) the mobility is not sufficient to form these ordered dislocation structures, as evident in the roughness seen in STM at 4.7 ML [26,27]; (ii) hysteresis curves of 4.7 ML films grown at 300 K [27] actually show the same coercivity for fields applied along the ⟨110⟩ and ⟨100⟩ directions. In fact, the saturation of the magnetization was much faster with increasing field along the

⟨110⟩ direction. This led to the conclusion that the easy axis is along ⟨110⟩ for growth at 300 K [26,27]. Earlier studies of up to 5-ML-thick [21] and 10-ML-thick [23] films also showed little difference between the hysteresis curves obtained with fields along the ⟨100⟩ and ⟨110⟩ directions. These somewhat inconclusive observations can now be considered in light of the detailed data shown in Fig. 7(c): $\boldsymbol{M}$ rotates away from the [110], not completely into the [010], direction ($\phi = 90^\circ$) but rather remains oriented significantly away from it ($\sim 10^\circ$) in the 3.9–4.9-ML-thickness range. This behavior at 300 K is incompatible with the model proposed earlier to account for the magnetization rotation at 400 K (i.e., that it is due to partial strain relaxation) [26,27]. Therefore, an alternative explanation must be sought to account for the incompatible behavior observed here in this thickness range at 300 K.

Interestingly, the asymmetry decreases abruptly beyond 3.9 ML, reaching a value as low as 0.037 at 4.9 ML [Fig. 7(b)], while the single domain state and the direction of $\boldsymbol{M}$ [Figs. 6(b) and 7(c)] persist from 3.9 ML up to at least 4.7 ML. Keeping the decrease of the magnetic moment that couples to the decreasing interatomic distance in mind [36], the decrease of the asymmetry between 3.9 and 4.9 ML at 300 K may actually signal a strong contraction normal to the surface starting at 3.9 ML. This contraction modifies the tetragonal distortion described earlier and induces a change in the magnitude of the magnetization that is seen in the reduction of the asymmetry without affecting the magnetization direction. This contraction and not the introduction of misfit dislocations should be responsible for the constant stress in this thickness range at 300 K.

At about 4.8 ML, new domains (cyan triangles in Fig. 7) suddenly form within the single domain (green squares in Fig. 7) that is initially present [Figs. 5(b)]. The new domains are elongated along step bunches originally seen in LEEM images of the clean surface. The magnetization within the new domains is initially aligned at $\phi \sim 150^\circ$ (i.e., at 45° relative to the magnetization direction in the single domain that was originally present—green squares in Fig. 7—which is aligned at $\phi \sim 105^\circ$). Simultaneously with the appearance of the new domains, the FWHM of the angular distribution of $\boldsymbol{M}$ increases significantly. As seen in Fig. 7(e), a significant part of the angular distribution also cannot be fit after the appearance of the new domains at 4.8 ML due to the serrated shape of the domains seen in the images (see Supplemental Material for details of the fitting procedure and additional results [33]). With increasing thickness, the size and number of these new domains increases rapidly so that at 5.1 ML, the two distinctly different domains cover equal fractions of the surface. Simultaneously the "fuzziness" of the domains increases, causing a strong increase of the nonfitted fraction of the film [Fig. 7(e)] and in the domain wall length [Fig. 7(f)]. The "fuzziness" and similarity of these two curves [Figs. 7(e) and 7(f)] suggests that the magnetic anisotropy is particularly small above 4.8 ML and continues to decrease up to about 6.7 ML. The magnetizations within the two domains also rotate abruptly in the same direction (i.e., positively in ϕ), initially between 4.8 and 5.1 ML. This is followed by somewhat more gradual rotations of the magnetizations in the two domains towards each other [green square/cyan triangle data points in Fig. 7(c)], approaching as close as $\phi = 130^\circ$ and 160°, respectively, at about 6.5 ML. These two directions do not correspond to any high symmetry directions. Earlier hysteresis curve measurements that did not have the high azimuthal angular resolution that we have here were simply interpreted as evidence of a ⟨110⟩ easy axis up to about 6 ML [27]. The complex behavior revealed here indicate that this interpretation may not be complete.

At about 7.0 ML, new domains appear (blue diamonds in Fig. 7) that grow rapidly with increasing thickness. The $\boldsymbol{M}$ direction within the new domains is initially close to the $[\bar{1}00]$ direction at $\phi = 180^\circ$, but rotates rapidly with increasing thickness to about 220° (i.e., close to the $[\bar{1}\,\bar{1}0]$ direction [Fig. 7(c)]). Correspondingly, the fractional coverages of the two pre-existing domains rapidly diminish with increasing thickness [green squares and cyan triangles in Fig. 7(a)]. Simultaneously, their $\boldsymbol{M}$ angular distributions broaden noticeably [Fig. 7(d)]. All three domains with distinct $\boldsymbol{M}$ directions above 7 ML exhibit interesting features. The final majority domain is strongly mottled in the magnetization direction image [e.g., Fig. 5(f4)] with patches aligned at $\phi \sim 200^\circ$ (light blue) interspersed in larger regions aligned at $\phi \sim 225^\circ$ (dark blue), indicating that the film is magnetically very soft. The $\boldsymbol{M}$ direction that had been dominating between 5 and 7 ML (cyan triangles in Fig. 7) rapidly disappears between 7 and 8 ML, while the initial orientation (green squares in Fig. 7) persists, with some rotation between 7 and 9 ML [Fig. 7(c)] in strongly elongated domains up to the largest thickness studied in this particular experiment. After the rotation, the $\boldsymbol{M}$ direction varies from the middle to the edge of these persistent domains, which can be seen in the magnetization direction image [Fig. 5(f4)] and in the broad overlapping tail on the left side of the $\boldsymbol{M}$ angular distribution histogram in Fig. 5(f5). Other experiments carried out up to a larger thickness show that the orientation of the persistent pinned domains (green squares) after rotation is stable up to the largest thickness, while the intermediate $\boldsymbol{M}$ orientation (cyan triangles) disappears, as illustrated in Fig. 11.

The dominating $\boldsymbol{M}$ orientation ends up close to the $[\bar{1}\,\bar{1}0]$ direction, $\phi = 225^\circ$, in the 8.8-ML-thick film shown in Figs. 5 and 7. Equivalent directions are observed in the thicker film [Figs. 11(b)] and are also reproducibly observed in thick films in other experiments [Figs. 11(a)]. This seems to be at variance with MOKE hysteresis measurements from which the ⟨100⟩ direction has been deduced as the easy axis above 6 ML [27]. This was concluded from the fact that saturation was reached already at 3 mT when the field was applied along the ⟨100⟩ direction, while saturation was not possible with field along the ⟨110⟩ direction within the available field range, although the coercivity along the ⟨100⟩ direction was significantly larger than along the ⟨110⟩ direction. It also has to be kept in mind that the easy axis in the virgin state can be compared only to a limited extent with the easy axis determined by applying a field. An example is the observation that the virgin state in a Co film could be regenerated only approximately by annealing after field application [37].

Another possible explanation of the difference between the virgin domain behavior studied here and the behavior revealed by the earlier MOKE hysteresis measurements could be that differences in the deposition conditions could result in different morphology, stress, and defects to which the magnetization easy axis is very sensitive. For instance, films were grown by

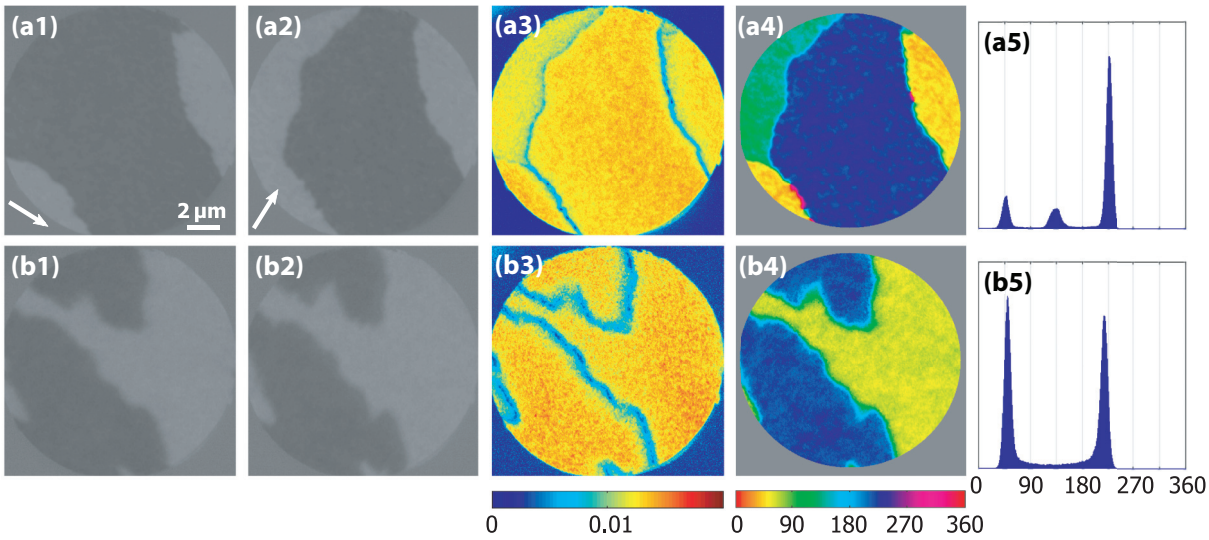

FIG. 11. SPLEEM images of films grown at room temperature. (a) 8 ML and (b) 9.8 ML. The figure shows from left to right: image taken with polarization (1) parallel to [100] direction, (2) parallel to [010] direction as arrows point, respectively; composite images that present (3) magnitude of the magnetic asymmetry and (4) magnetization direction; and (5) histogram of the angular distribution of the magnetization direction calculated pixel by pixel from (4). The imaging electron energy is 0.5 eV.

Fe deposition at normal incidence in the earlier work, whereas the Fe vapor beam had an angle of incidence of 74° from the sample normal here. This oblique incidence could lead with increasing deposition time to the formation of ripples perpendicular the direction of the vapor beam that would introduce some shape anisotropy with the easy axis along the ripple direction [38,39]. However, we can rule out such oblique incidence growth-induced ripple morphology here as the origin of the $[\bar{1}\,\bar{1}0]$-oriented magnetization in thick films ($\geqslant$8 ML) because domains with an easy axis along the $[\bar{1}10]$ axis, orthogonal to the easy axis shown in Figs. 5(f) and 7(c), were also observed in other thick films in our investigations, although the deposition azimuth was not changed [Figs. 11(a)]. The only effect of the large angle of incidence is the faster growth on step bunches pointing at the evaporator, which led to the earlier transition to new $\boldsymbol{M}$ direction with increasing thickness. However the direction of the step bunches varies locally, and no correlation with the $\boldsymbol{M}$ direction was observed.

During all these complex changes of the domain structure and magnetization direction at room temperature, the exchange asymmetry remains approximately constant after the sudden decrease connected with growth of the fifth monolayer [Figs. 6(a) and 7(b)]. The quasiperiodic oscillations of the asymmetry around the mean value of about 0.035 above 6 ML could in principle be quantum size oscillations; however, the increasing roughness of the film in this thickness range makes such an interpretation unlikely. An experimental artifact cannot be excluded.

Summarizing this section, the detailed SPLEEM measurements that are presented here were made with intrinsically better azimuthal angular and film thickness resolutions than earlier studies of Fe films grown on the W(001) surface at room temperature. These detailed studies reveal a different and more complex picture than was evident in earlier investigations. Fe films grown on the W(001) surface at room temperature exhibit a sequence of domain configurations with strongly varying magnetization direction and domain shapes and sizes. The magnetization direction is in general not along one of the high symmetry directions of Fe. A number of possible influences have been considered, including tetragonal distortion of the unit cell, changing spin state upon strain relaxation by further vertical contraction of the tetragonal film, coupling of magnetostrictive effects with anisotropy of in-plane elastic properties of the film, and shape anisotropy related to island morphology of the rough film, as well as substrate step morphology. The nature of the domain walls and the internal structure of the domains indicate weak magnetic anisotropy, except in the 4-ML-thick tetragonal film, which forms a single domain state. These observations explain the early conflicting reports of a different easy axis and shed additional light on the insignificant magnetic anisotropy.

B. Growth at elevated temperatures

The growth above room temperature was studied with LEEM to understand how the interesting complicated morphological structures observed earlier with STM at intermediate temperatures (360–550 K) develop with increasing thickness [26,27,29,30]. The LEEM movies presented here illustrate the growth at selected temperatures, 700, 600, 500, and 400 K, respectively, although with much poorer resolution than the earlier STM studies (see Supplemental Material for LEEM movies [33]). Movies of growth at 400 and 450 K show no clear signs of the linear and cross-patterned island structures that were seen with STM in this temperature range, possibly due to the limited LEEM resolution. The LEEM movies instead only show an increase in particle density above about 3.6 ML. Clear signs of nucleation that triggers the partial dewetting of a nearly 4-ML-thick film, however, are visible during the growth at 500 K [Fig. 3(c)], although the internal

structure of the islands that form at this temperature is still difficult to resolve with LEEM. However, the cross-shaped patterns within nucleated islands that were reported in the STM studies could be observed in SPLEEM measurements at 500 K, noting the concern about comparing temperatures in different setups [Fig. 4(b)]. The nucleation of thin short wires was clearly resolved with LEEM during growth at 600 K that triggers partial dewetting of the surrounding film already at 3.21 ML [Fig. 3(b) and 4(a)]. Three-dimensional crystals form at the ends of these wires with further growth. During growth at 700 K, the nucleation of 3D compact isometric crystals is observed already at 2.63 ML [Fig. 3(a)], which triggers either dewetting of a condensed layer or a reduction of the density of a coexisting 2D gas of Fe adatoms. These results agree qualitatively with the STM results, keeping in mind the difficulties of temperature measurement and different deposition conditions. These investigations extend the temperature range for observations of the Fe growth mode, elaborate on the transitions between growth modes with increasing temperature, and show the dynamics of the growth itself in full detail.

An important comparison can be made between the growth and morphology of Fe on W(001) and corresponding behavior of Cr on W(001) that was studied earlier [40,41]. Fe and Cr are both bcc with nearly identical lattice mismatch, ∼10%, from W. In both cases, growth of highly (tensile) strained pseudomorphic films occurs at an elevated temperature initially. Likewise, 3D island nucleation triggers dewetting of material in excess of the thermodynamically stable wetting layers in both cases. Although the strain is nearly the same for the pseudomorphic Fe and Cr films, 3D island nucleation and dewetting occur at different metastable film thicknesses in the two cases: nearly 4 ML for Fe/W(001) compared with only 3 ML for Cr/W(001). This difference may be due to the fact that the strain energy of Cr is higher than Fe for the same strain. In particular, the strain energy of a film is proportional to its shear modulus, which is higher for bulk Cr, 115 GPa, than for bulk Fe, 82 GPa [42,43]. The formation of dislocation networks in Fe/W(001) during growth at intermediate temperature, but their absence in Cr/W(001), was also attributed to the different strain energies in pseudomorphic Cr and Fe films [41], although this connection is less obvious than between strain energy and the onset of 3D island nucleation and dewetting. The 3D island morphologies formed by Cr and Fe following dewetting are also dramatically different. Compact Fe islands form on W(100) at elevated temperature with Fe [001]$\|$W[001] [the (001) planes of W and Fe are parallel] and with {310} top facets. On the contrary, the (001) planes in Cr islands are tilted by ∼5° with respect to the substrate (001) planes; these islands are bounded by {211} side facets and (001) top facets that are correspondingly tilted. The tilting of the Cr crystallite generates a high-index interfacial Cr plane parallel to the substrate that effectively creates a pseudovicinal interface. Such a configuration may accommodate strain and avoid the introduction of misfit dislocations [44]. The absence of similar phenomena in the 3D island morphology of Fe/W(001) leads us to speculate that dislocations may be present at the interface of Fe islands on W(001) that play a role in accommodating lattice mismatch between island and substrate.

Another aim of this study was to clarify how growth temperature affects the magnetic domain structure. The domain structure of films grown at 400 K differs significantly from that of films grown at 300 K, as shown in Figs. 5 and 8. During growth at 300 K, the magnetization is oriented close to the [$\bar{1}$10] direction with narrow angular distribution shortly after onset at ∼3 ML thickness [Figs. 6(b), 7(c), and 7(d)]. The magnetization direction then rotates continuously from [$\bar{1}$10] to near [010] between 3 and 4 ML during growth at 300 K. On the contrary, a multidomain state with a broad $\boldsymbol{M}$ angular distribution near to preferred ⟨100⟩ directions is present already at the outset in the 3 ML film grown at 400 K [Figs. 8(a)], avoiding the initial ⟨110⟩ orientation. At 4 ML, the magnetization directions and domain structures observed during growth at 300 and 400 K are similar to each other [compare Figs. 5(b) and 8(b), in which several domains with different ⟨100⟩$\boldsymbol{M}$ directions are in the field of view]. The initial differences in 3 ML films can be correlated with differences in the film morphology at the two temperatures. As discussed earlier, at 300 K, the 3 ML film consists of a mixture of 2-, 3-, and 4-ML-thick regions, with the 3 ML regions only partially covering the surface. The origin of the [$\bar{1}$10]-oriented easy axis in the 3 ML film with this morphology is not fully understood, but the rotation towards the [100] direction does coincide with greater filling of the third layer.

The higher mobility at 400 K leads to the completion of the 2 ML film before any significant growth of the third layer occurs (Fig. 1). While not perfect, the morphology of the 3 ML film grown at 400 K is still much more uniform than at 300 K. The wide magnetization angular distribution is present along ⟨100⟩ directions in the smoother 3 ML film at 400 K because of an apparently weak intrinsic anisotropy [Figs. 8(a)]. The distribution narrows considerably due to strengthening anisotropy during the growth of the fourth layer at 400 K [Figs. 8(b)].

Significant changes in the domain structure occur above 4 ML at 300 and 400 K. While the evolution from the large, single domain state at 3.9 ML to the multidomain state above 4.7 ML can be followed clearly in the film grown at 300 K in great detail by cumulative deposition (Figs. 5–7; also see Supplemental Material [33]), it was not possible to follow the dramatic transition between 4 and 5 ML in films grown at 400 K in the same way because of sample drift that occurred when the sample was cooled to room temperature for measurement. Nevertheless, we see that several large domains remain in 5 and 6 ML films grown at 400 K that now all exhibit pronounced elongated substructure with preferred direction related to the dominant $\boldsymbol{M}$ direction in the domains. This leads to the broad angular distribution seen in the histograms [Figs. 8(c5) and 8(d5)], which now have their maxima in the ⟨110⟩ directions at both thicknesses. At 300 K, kinetic limitations lead to a delayed, more complicated two-stage spin reorientation transition with sudden onsets: one at about 4.9 ML (cyan triangles in Fig. 7) and the second at about 7 ML (blue diamonds in Fig. 7). The dominant final $\boldsymbol{M}$ direction at 300 K is also along ⟨110⟩, but with less internal direction fluctuations and with imbedded elongated domains, whose $\boldsymbol{M}$ direction is near [100]. Overall, comparison of the magnetic evolution of films grown at 300 and 400 K clearly shows underlying common features. At both temperatures, large

domains with pronounced $\boldsymbol{M}$ alignment in ⟨100⟩ directions in the tetragonal film at 4 ML eventually transform with increasing thickness into domains with poorer $\boldsymbol{M}$ alignment, predominantly in ⟨110⟩ directions in the thickest films. As the inelastic mean free path of the electrons, though small [45], is long enough to sample the magnetization of deeper layers in 5- and 6-ML-thick films, this observation indicates that the high spin phase of the 4 ML film is converted into the lower spin phase of less well ordered thicker films that have weaker magnetic anisotropy and ⟨110⟩ easy axes.

As discussed earlier, dewetting during growth at 600 K starts already at 3.21 ML, leading to 3D crystals surrounded by 2 ML regions and 3- and 4-ML-thick islands before all material in excess of 2 ML has been converted into 3D crystals (see Supplemental Material for LEEM Movie S3 [33]). The $\boldsymbol{M}$ directions and angular distributions in the smooth 4 ML regions and 3 ML regions that are exposed during dewetting at 600 K are very similar to those of continuous films that are grown directly to these thicknesses at 400 K. In particular, $\boldsymbol{M}$ is very narrowly distributed parallel to the [100] direction in a single domain state at 4 and 3 ML exhibits a state with $\boldsymbol{M}$ also preferentially close to ⟨100⟩ directions but with considerably wider angular distribution [Figs. 9(e), 9(f), and 9(h)]. The clusters of interconnected 3D crystals that form during dewetting at 600 K, however, show a complex $\boldsymbol{M}$ pattern, depending upon their specific interconnection and shape [Fig. 9(g)] but with no apparent magnetic closure in the clusters, resulting in a wide, almost isotropic, angular distribution of $\boldsymbol{M}$ [Fig. 9(h)]. In contrast, the isolated crystals with square and rectangular cross section that grow directly on top of the nonmagnetic double layer at 700 K have simple magnetic domain patterns (Fig. 10): vortex [Figs. 10(d)–10(g)] and *C*-state [Figs. 10(h)–10(k)] patterns in sufficiently large (several 100 nm edge lengths) square and rectangular crystals, single domain states [Figs. 10(l)–10(o)] in smaller crystals (about 100 nm edge lengths). Thus the $\boldsymbol{M}$ distribution in the crystals is completely determined by the shape anisotropy of a material with weak crystal anisotropy as calculated by Hertel [46] with micromagnetic simulations and confirmed experimentally for lithographically prepared Co thin film patterns [47].

The current investigations provide further insight into the relationship between magnetism of thin films and particles on macroscopic surfaces and the spin polarization of field-emitted electrons from Fe-covered W(001)-oriented tips [31,32]. The spin polarization of field-emitted electrons from Fe/W(001) tips was determined to be along transverse ⟨100⟩ directions. Following Fe deposition at 300 K, the onset of polarization was detected between 6 and 7 ML (based on quartz crystal oscillator calibration) at 300 K. Rapid fluctuations of polarization direction among four possible transverse ⟨100⟩ directions were observed at the onset that gradually diminished in frequency with increasing Fe deposition. Furthermore, the transverse polarization in ⟨100⟩ directions persisted up to the maximum deposited thickness studied, >9 ML. Temperature-dependent fluctuations between ⟨100⟩ directions were also observed for different fixed Fe tip coverages. These behaviors were attributed to superparamagnetic fluctuations of the tip magnetization direction. The observed tip magnetization directions are consistent to some extent with the magnetization easy axis nearly aligned with the ⟨100⟩ directions [Figs. 6(b) and 7(c)] in ∼4–5-ML-thick films on a macroscopic W(001) crystal that were deposited at room temperature in this work. However, the tip magnetization onset thickness and the persistent tip magnetization along ⟨100⟩ directions at larger deposited thickness obviously differ significantly from the behavior exhibited by films on a macroscopic W(001) surface. Rather, the emitting object on Fe-coated tips may be more reasonably likened to compact, relaxed 3D Fe islands on W(001), which exhibit precisely aligned in-plane ⟨100⟩ magnetization. The estimated Fe particle size on the end of the W(001) tip that gives rise to spin-polarized field emission [31] falls into the regime that single-domain 3D islands were found on a macroscopic W(001) surface in another paper [28]. Due to the lateral confinement of the tip, Fe deposition on a W(001) tip only increases the 3D island height, not its width. This insight also suggests that the formation of (111)-oriented 3D crystals is responsible for producing similar superparamagnetic fluctuations in spin-polarized field emission from Fe- and Co-coated W(111) tips [32,48].

V. SUMMARY

This real-time LEEM and quasi-real-time SPLEEM study provides detailed information about the growth and morphological and magnetic evolution of Fe films on W(001) up to about 10 ML thickness with high thickness, lateral and azimuthal angular resolution. Our investigations reveal that the magnetic evolution of the system is much more complex than reported previously on the basis of laterally averaging and laterally resolving magnetic measurements that were made only at selected thicknesses and with limited angular resolution. We find that the dominant magnetization direction in the virgin state studied here at room temperature is in general not precisely in any of the high symmetry directions. It rotates from near the ⟨110⟩ direction at 3 ML shortly after the onset of magnetism to near ⟨100⟩ at around 4 ML, after which it changes via a complex process with increasing thickness to near the ⟨110⟩ direction beyond 8 ML. This contrasts with the preferred magnetization direction (i.e., easy axis) that was deduced in the ⟨110⟩ direction up to 6 ML and in the ⟨100⟩ direction at larger thicknesses from MOKE measurements [26,27]. The differences of our results from the earlier MOKE results may be attributed to domain wall pinning during cycling of an applied field during MOKE hysteresis measurements, although differences in the microstructure of the films cannot be excluded as possible causes. The initial magnetization direction near ⟨110⟩ observed in our work and reported in some of the earlier papers is already established at low thickness, while the film still consists of individual islands, whose interactions must play a role in determining the magnetization direction. However, the final magnetization direction determined in thick films here is not consistent with the easy axes of bulk Fe, namely the ⟨100⟩ direction, and must be attributed to strain and the poor order of the film. In the regimes of low or high thickness mentioned above, the domain structure indicates that the magnetic anisotropy is weak, in agreement with some earlier reports [20,21,23,24,26,27]. The presence of such a weak anisotropy may account for the discrepancies about the easy axes determined by other

techniques in earlier papers [20,23,26,27]. On the other hand, the magnetization signal strength and its very narrow alignment near the [100] direction that are determined at 4 ML here provide evidence of a significantly higher magnetic moment and significant anisotropy at this coverage that leads to large domains. The magnetic evolution at 400 K is overall similar to that at room temperature, except that the initial magnetization direction is already along ⟨100⟩ instead of ⟨110⟩ at 3 ML at this temperature, so that the first magnetic reorientation that occurs between 3 and 4 ML at 300 K is absent at 400 K. This key difference between films deposited at 300 and 400 K is ascribed to the film morphology, namely a greater filling of the third layer at 400 K. In agreement with earlier papers, the tetragonally distorted epitaxial 4-ML-thick film is metastable and restructures at higher thickness into 3D crystals on top of a stable 2-ML-thick wetting layer at higher temperatures (i.e., 500–700 K), a process vividly illustrated by LEEM movies of the growth. At about 600 K, this process leads to 3D crystals surrounded by 2 ML regions and 3- and 4-ML-thick islands. The 3D crystals here show very complex magnetic structures with a wide almost isotropic angular distribution of magnetization because of their small size and interconnection, while the isolated 3D Fe crystals grown at 700 K indeed have well-defined magnetic structures depending on their shape and size. The 3 and 4 ML areas grown at about 600 K, though similar to their counterparts grown at 400 K in term of magnetic structures and easy axis, have higher magnetic asymmetry, which is clearly due to a much better order of Fe films. In many respects, the Fe/W(001) system seems very sensitive and unusual and deserves further studies without and with applied magnetic field.

ACKNOWLEDGMENT

This work was financially supported by the Hong Kong Research Grants Council, University Grants Committee (Grant No. 600110).

[1] D. Sander, J. Phys.: Condens. Matter **16**, R603 (2004).
[2] P. J. Jensen and K. H. Bennemann, Surf. Sci. Rep. **61**, 129 (2006).
[3] C. A. F. Vaz, J. A. C. Bland, and G. Lauhoff, Rep. Prog. Phys. **71**, 056501 (2008).
[4] A. Enders, R. Skomski, and J. Honolka, J. Phys.: Condens. Matter **22**, 433001 (2010).
[5] J. Hauschild, H. J. Elmers, and U. Gradmann, Phys. Rev. B **57**, R677 (1998).
[6] H. J. Elmers, J. Hauschild, H. Höche, U. Gradmann, H. Bethge, D. Heuer, and U. Köhler, Phys. Rev. Lett. **73**, 898 (1994).
[7] H. L. Meyerheim, J.-M. Tonnerre, L. Sandratskii, H. C. N. Tolentino, M. Przybylski, Y. Gabi, F. Yildiz, X. L. Fu, E. Bontempi, S. Grenier *et al.*, Phys. Rev. Lett. **103**, 267202 (2009).
[8] Y. Tsunoda, J. Phys.: Condens. Matter **1**, 10427 (1989).
[9] K. Zakeri, T. Kebe, J. Lindner, and M. Farle, J. Magn. Magn. Mater. **299**, L1 (2006).
[10] A. Maziewski, J. Fassbender, J. Kisielewski, M. Kisielewski, Z. Kurant, P. Mazalski, F. Stobiecki, A. Stupakiewicz, I. Sveklo, M. Tekielak *et al.*, Phys. Status Solidi A **211**, 1005 (2014).
[11] T. Ślęzak, M. Ślęzak, M. Zając, K. Freindl, A. Kozioł-Rachwał, K. Matlak, N. Spiridis, D. Wilgocka-Ślęzak, E. Partyka-Jankowska, M. Rennhofer, A. I. Chumakov, S. Stankov, R. Ruffer, and J. Korecki, Phys. Rev. Lett. **105**, 027206 (2010).
[12] E. Bauer, Rep. Prog. Phys. **57**, 895 (1994).
[13] E. Bauer, *Surface Microscopy with Low Energy Electrons* (Springer-Verlag, New York, 2014), p. 496.
[14] M. S. Altman, J. Phys.: Condens. Matter **22**, 084017 (2010).
[15] N. Rougemaille and A. K. Schmid, Eur. Phys. J. Appl. Phys. **50**, 20101 (2010).
[16] T. M. Gardiner, Thin Solid Films **105**, 213 (1983).
[17] X. L. Zhou, C. Yoon, and J. M. White, Surf. Sci. **203**, 53 (1988).
[18] P. J. Berlowitz, J. W. He, and D. W. Goodman, Surf. Sci. **231**, 315 (1990).
[19] R. L. Fink, G. A. Mulhollan, A. B. Andrews, J. L. Erskine, and G. K. Walters, J. Appl. Phys. **69**, 4986 (1991).
[20] G. A. Mulhollan, R. L. Fink, J. L. Erskine, and G. K. Walters, Phys. Rev. B **43**, 13645 (1991).
[21] J. Chen and J. L. Erskine, Phys. Rev. Lett. **68**, 1212 (1992).
[22] H. J. Elmers and J. Hauschild, Surf. Sci. **320**, 134 (1994).
[23] T. L. Jones and D. Venus, Surf. Sci. **302**, 126 (1994).
[24] H. J. Choi, R. K. Kawakami, E. J. Escorcia-Aparicio, Z. Q. Qiu, J. Pearson, J. S. Jiang, D. Li, R. M. Osgood, and S. D. Bader, J. Appl. Phys. **85**, 4958 (1999).
[25] A. Enders, D. Sander, and J. Kirschner, J. Appl. Phys. **85**, 5279 (1999).
[26] W. Wulfhekel, F. Zavaliche, F. Porrati, H. P. Oepen, and J. Kirschner, Europhys. Lett. **49**, 651 (2000).
[27] W. Wulfhekel, F. Zavaliche, R. Hertel, S. Bodea, G. Steierl, G. Liu, J. Kirschner, and H. P. Oepen, Phys. Rev. B **68**, 144416 (2003).
[28] A. Yamasaki, W. Wulfhekel, R. Hertel, S. Suga, and J. Kirschner, Phys. Rev. Lett. **91**, 127201 (2003).
[29] K. von Bergmann, M. Bode, and R. Wiesendanger, Phys. Rev. B **70**, 174455 (2004).
[30] K. von Bergmann, M. Bode, A. Kubetzka, O. Pietzsch, and R. Wiesendanger, Microsc. Res. Techniq. **66**, 61 (2005).
[31] Y. R. Niu and M. S. Altman, Appl. Phys. Lett. **95**, 203113 (2009).
[32] Y. R. Niu and M. S. Altman, Surf. Sci. **604**, 1055 (2010).
[33] See Supplemental Material at http://link.aps.org/supplemental/10.1103/PhysRevB.95.064404 for SPLEEM movies, further details of the experimental data, and analyses.
[34] W. X. Tang, K. L. Man, H. Huang, C. H. Woo, and M. S. Altman, J. Vac. Sci. Technol. B **20**, 2492 (2002).
[35] P. Błoński and A. Kiejna, Surf. Sci. **601**, 123 (2007).
[36] H. Wang, P.-W. Ma, and C. H. Woo, Phys. Rev. B **82**, 144304 (2010).
[37] M. Speckmann, H. P. Oepen, and H. Ibach, Phys. Rev. Lett. **75**, 2035 (1995).
[38] Q. Zhan, C. Van Haesendonck, S. Vandezande, and K. Temst, Appl. Phys. Lett. **94**, 042504 (2009).
[39] F. L. W. Rabbering, G. Stoian, R. van Gastel, H. Wormeester, and B. Poelsema, Phys. Rev. B **81**, 115425 (2010).
[40] K. L. Man, Q. Guo, and M. S. Altman, Surf. Sci. **600**, 1060 (2006).

[41] R. A. Bennett, J. S. Mulley, H. A. Etman, A. Sparkes, T. Eralp, G. Held, S. A. Cavill, and S. S. Dhesi, Phys. Rev. B **86**, 045454 (2012).

[42] P. Enghag, *Encyclopedia of the Elements: Technical Data—History—Processing–Applications* (Wiley, Weinheim, 2008).

[43] The strain energy in the pseudomorphic layer with a thickness of h was assumed to be $E_e = 2Gh f^2(1+\upsilon)(1-\upsilon)$, where G is the shear modulus, f the lattice mismatch, and υ the Poisson ratio. See J. E. Ayers, *Heteroepitaxy of Semiconductors* (CRC Press, Boca Raton, FL, 2007), Chap. 5, p. 161.

[44] J. H. van der Merwe and G. J. Shiflet, Acta Metall. Mater. **42**, 1173 (1994).

[45] R. Zdyb and E. Bauer, J. Phys.: Condens. Matter **25**, 272201 (2013).

[46] R. Hertel, Z. Metallkd. **93**, 957 (2002).

[47] S. Cherifi, R. Hertel, J. Kirschner, H. Wang, R. Belkhou, A. Locatelli, S. Heun, A. Pavlovska, and E. Bauer, J. Appl. Phys. **98**, 043901 (2005).

[48] R. Bryl and M. S. Altman, J. Appl. Phys. **94**, 4670 (2003).